Research Article | Vol. 9, No. 10 / 1 October 2019 / Optical Materials Express 4126
Optical Materials EXPRESS

Fluorescence intensity ratio and whispering gallery mode techniques in optical temperature sensors: comparative study

F. Paz-Buclatin,[1,*] S. Ríos,[1] I. R. Martín,[1,2] and L. L. Martin[1]

[1] Departamento de Física, Universidad de La Laguna. Apdo. 456. E-38200 San Cristóbal de La Laguna, Santa Cruz de Tenerife, Spain
[2] Instituto Universitario de Materiales y Nanotecnología (IMN), Universidad de La Laguna. Apdo. 456. E-38200 San Cristóbal de La Laguna, Santa Cruz de Tenerife, Spain
[*] fpazbucl@ull.es

Abstract: The thermal sensing capabilities of different morphologies (microsphere, fiber, and bulk glass) of an Er^{3+} doped oxyfluoride glass were characterized in order to determine the most suitable material to be developed as a temperature sensor. For the microsphere and fiber, the displacements of the whispering gallery mode peaks were correlated with the temperature change. The thermal expansion and thermo-optic coefficient of the bulk glass were measured for the numerical simulations of the WGM shift with temperature. On the other hand, a fluorescence intensity ratio technique was used to estimate the temperature of the bulk glass. In order to compare the sensor performance of each sample, the relative sensitivity and temperature uncertainty were determined.

1. Introduction

Optical sensors operate by detecting changes in the intensity, phase, polarization, wavelength or spectral distribution of the light beams as they interact with the surrounding medium. This type of sensor usually provides more efficiency due to their exclusive features accounting from their light-based detection mechanism [1]. Unlike electronic sensors, optical sensors offer electrical passiveness, immunity from electromagnetic interference, large bandwidth, both point and distributed configurations and multiplexing capabilities [2]. Moreover, optical sensors in the form of fluorescent nanoparticles and microspheres permit non-invasive measurements through non-contact sensing mechanisms. In this way, the sensor is deposited into the sample, an external perturbation is made, and the sensor's response is detected externally [3].

Rare earth ions, particularly in their trivalent form, are usually employed in the development of optical sensors due to their interesting optical properties. They are relatively easily obtainable and their absorption bands are within the emission spectrum of readily available pump sources. Additionally, they present prominent transition lines in the visible and near infrared region and due to the screening of outer electrons, their energy level structure only varies slightly between different host materials [4]. They also have thermally coupled levels which are of interest for the Fluorescence Intensity Ratio (FIR) technique. Particularly, the Er^{3+} ion has the thermally coupled $^2H_{11/2}$ and $^4S_{3/2}$ levels. It is one of the most used rare earth ions due to its applications as a fiber amplifier for the 1.5 μm telecommunication range [5]. Moreover, it presents emission lines in the near infrared region where the biological tissue is transparent, thus, it can also be used in biomedicine.

In the design of optical devices, the host material is also an important factor to consider since their vibrational properties can influence the optical behavior of the dopant ion. Many of the transition lines of practical importance of rare earth ions originate from excited levels with a

#373962 https://doi.org/10.1364/OME.9.004126
Journal © 2019 Received 1 Aug 2019; revised 20 Sep 2019; accepted 20 Sep 2019; published 26 Sep 2019

Optical Materials EXPRESS

relatively small energy gap, from 200 cm^{-1} to 2000 cm^{-1} in the case of thermally coupled levels studied in the FIR technique. Therefore, in order for the radiative transitions of the active ions to dominate the non-radiative loss, materials with lower phonon energy are recommended as hosts such as fluoride glasses (300–400 cm^{-1}). However, because of their low chemical and mechanical stabilities, fluoride glasses are difficult to fabricate. On the other hand, oxide glasses have better chemical and mechanical stabilities but higher phonon energy (1100 cm^{-1}). Thus, oxyfluoride glasses are expected to have excellent optical properties and good mechanical and chemical stability resulting from the compromise between pure fluoride and oxide glasses [6,7].

With this in mind, the main objective of this work is to study the potential of an Er^{3+} doped oxyfluoride glass as an optical temperature sensor. Two techniques are usually employed, the study of Whispering Gallery Modes (WGM) displacements when using a microresonator [8–11] and the FIR technique when using lanthanide-doped materials [12–14]. In this work, a comparative study of the efficiency of each technique for the same Er^{3+} doped precursor glass was performed.

2. Theoretical background

2.1. WGM displacement technique

WGM are a family of morphology dependent resonances of a wave field inside a cavity due to the successive total internal reflections on a circular section. The optical modes of a resonator can be calculated analytically by solving the Helmholtz equation at the resonator-medium boundary in spherical or cylindrical coordinates, depending on the geometry of the resonator [15]. It can also be studied through a geometrical approximation valid for a large number of wavelengths in the circumference, represented by the parameter l, also known as the polar mode number. For a resonator of radius R greater than the wavelength λ, a constructive interference occurs when the condition $2\pi Rn = l\lambda$ is met where n is the refractive index [16].

The size and refractive index of the resonator can vary depending on the thermodynamic conditions of its surrounding medium, such as temperature, pressure, or humidity. These changes will be reflected on the resonant wavelength, being the reason why they are often used as thermal [8–10], pressure [17], or humidity sensors [18] among others. The dependence of the displacement of the resonant wavelength with the temperature change ΔT is given as:

$$\Delta\lambda = \left(\frac{1}{R}\frac{\partial R}{\partial T} + \frac{1}{n}\frac{\partial n}{\partial T}\right)\lambda\Delta T \tag{1}$$

where T is the temperature.

Identifying $(1/R)(\partial R/\partial T)$ as the thermal expansion coefficient α and $(1/n)(\partial n/\partial T)$ as the thermo-optic coefficient β of the material, a more explicit expression describing the WGM displacements can be derived from Eq. (1) as follows:

$$\Delta\lambda = (\alpha + \beta)\lambda\Delta T \tag{2}$$

Since both coefficients are generally positive for glasses [19,20] a redshift of the resonant peaks as the temperature increases is expected as can be seen in Fig. 1(a) obtained from samples prepared by the authors. This technique relies on this peak shift in order to determine the temperature of the surrounding medium. Thus, it can only be used for microresonators that geometrically support WGM, such as microspheres, optical fibers, micro-toroid, and micro-disk among others.

2.2. Fluorescence intensity ratio

The FIR technique consists of analyzing the fluorescence intensity of thermally coupled energy levels to determine the temperature of the material. These thermally coupled energy levels are closely separated and are in thermal equilibrium. Due to the small energy gap between these levels, the atoms in the lower level can be promoted to the upper level with the increase of

Optical Materials EXPRESS

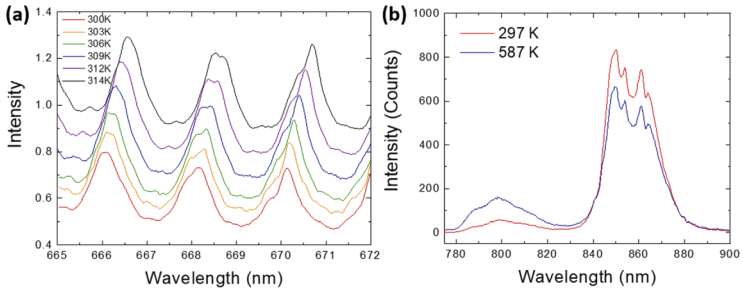

Fig. 1. (a) Shift of WGM peaks with increasing temperature for an Er^{3+} doped oxyfluoride microsphere with a radius of 35 μm and the (b) change in relative spectrum intensities for the 800 nm and 850 nm emission bands of Er^{3+} ions for two different temperatures in a bulk glass of the same material.

temperature through non-radiative mechanisms. Thus, the relative population of the upper and lower level changes such that the intensity of the emission band associated with the transition from the upper level increases, while that from the lower level decreases as can be seen in Fig. 1(b) where the 800 nm band corresponds to the former and the 850 nm band to the latter. This thermal redistribution of population follows the Boltzmann distribution given by the following equation [13,21]:

$$FIR = \frac{N_2}{N_1} = \frac{I_{20}}{I_{10}} = \frac{g_2 A_{20} h\nu_2}{g_1 A_{10} h\nu_1} \exp\left(-\frac{\Delta E}{kT}\right) = B \exp\left(-\frac{\Delta E}{kT}\right); B = \frac{g_2 A_{20} h\nu_2}{g_1 A_{10} h\nu_1} \tag{3}$$

where N_i, I_{i0}, g_i, A_{i0}, ν_i are the population, the fluorescence intensity, the degeneracy, the spontaneous emission rate and the angular frequency of the transition from the lower ($i = 1$) and upper ($i = 2$) thermally coupled levels to the terminal level 0, respectively; ΔE is the energy gap, h is the Planck's constant, k is the Boltzmann constant, and T is the absolute temperature of the material.

2.3. Sensor performance

Temperature sensor performance is usually described through the relative sensitivity and temperature uncertainty. In general, the relative sensitivity is defined as the rate at which the measured parameter (MP) changes due to a variation in temperature relative to the MP itself and is defined as [9]:

$$S_{rel} = \frac{1}{MP}\frac{d\,MP}{dT} \tag{4}$$

This figure of merit allows the comparison between thermometers of different nature, operating by different physical principles, or operating by the same physical principles but using different materials.

For a thermal sensor based on the WGM displacements, MP corresponds to the resonant wavelength and for one based on FIR, it corresponds to the intensity ratio. Using Eqs. (2) and (3), more straightforward expressions for the relative sensitivities are obtained:

$$S_{WGM} = \frac{1}{\lambda}\frac{d\lambda}{dT} = \alpha + \beta \tag{5}$$

$$S_{FIR} = \frac{1}{FIR}\frac{dFIR}{dT} = \frac{\Delta E}{kT^2} \tag{6}$$

On the other hand, the temperature uncertainty refers to the minimum temperature change that can be detected in a given measurement. Assuming that this change originates only from the

Optical Materials EXPRESS

changes in the measured parameter, δT is given by the following expression:

$$\delta T = \frac{1}{S_{rel}} \frac{\delta MP}{MP} \tag{7}$$

where δMP refers to the uncertainty of the measured parameter. This shows that δT is a function of the physical phenomena behind the sensor operation, quantified by S_{rel} and by the experimental setup.

Temperature uncertainties can be experimentally estimated by measuring MP several times under the same conditions, calculating each corresponding temperature and studying their statistical distribution [22].

3. Experimental methods

3.1. Production of Er^{3+} doped samples

All the samples studied in this work were obtained from the same matrix of Er^{3+} doped oxyfluoride glass with the following composition in mol%: 30 SiO_2, 15 Al_2O_3, 29 CdF_2, 22 PbF_2, 1.5 YF_3, and 2.5 ErF_3 [23].

The glass was produced by melting the precursor component at 1050°C for two hours in a platinum crucible and then the molten glass was poured onto a stainless-steel plate at room temperature to solidify resulting in a refractive index of about 1.75 [24]. The bulk glass will be further characterized in this work in terms of the thermal expansion coefficient α and the thermo-optic coefficient β obtaining that $\alpha = 13.0 \times 10^{-6}$ K^{-1} and $\beta = 5.9 \times 10^{-6}$ K^{-1}. Other parameters for a similar glass can be found in [24].

The fiber was produced by melting the glass matrix in a tubular furnace and continuously depositing it onto a rotating mechanism. In this way the melt is stretched, and the cylindrical form of the fiber is obtained.

The microspheres were obtained by rapid quenching of liquid droplets. The bulk glass was crushed and dropped into a flame. As the crushed glass melts, the surface tension molds it into a sphere which then transforms into an amorphous solid as it reaches the cooler region [25]. This fabrication process has no control over the microsphere size. In our case we obtained microspheres with radii ranging from 15 µm to 40 µm. The quality factor (Q), defined as the ratio of the peak wavelength and its width, ranges from 2000 - 4000. Figure 2 shows the fabricated microspheres with different sizes and a fiber with a radius of 41 µm under a microscope. For the experiment, a microsphere with a similar radius to the fiber (35 µm) and relatively high Q factor was chosen.

3.2. WGM displacement correlation

The emission spectra of the samples were obtained using a modified confocal microscope detailed in [26]. A continuous 532 nm DPSSL was used in order to excite the sample and the luminescent emission is detected using two different spectrographs, an SR-303i-B coupled with a Newton 970EMCCD camera for the visible region and an SR-500i-B2 coupled with an Andor iDusInGaAs photodiode array for the infrared region with wavelength resolutions of 0.1 nm and 0.05 nm, respectively. The setup permits changing the detection zone from the excitation zone. As reported by Martín et al. [26], the highest WGM resonance amplitudes were obtained by exciting at the center of the sample and detecting at its surface.

Using this setup, the samples were heated in two ways: by increasing the laser power and by using a thermal bath [8]. These permit the correlation of the WGM peak shifts with the temperature change. However, the correlation using the thermal bath was not done for the fiber due to the low contrast of the WGM peaks.

Optical Materials EXPRESS

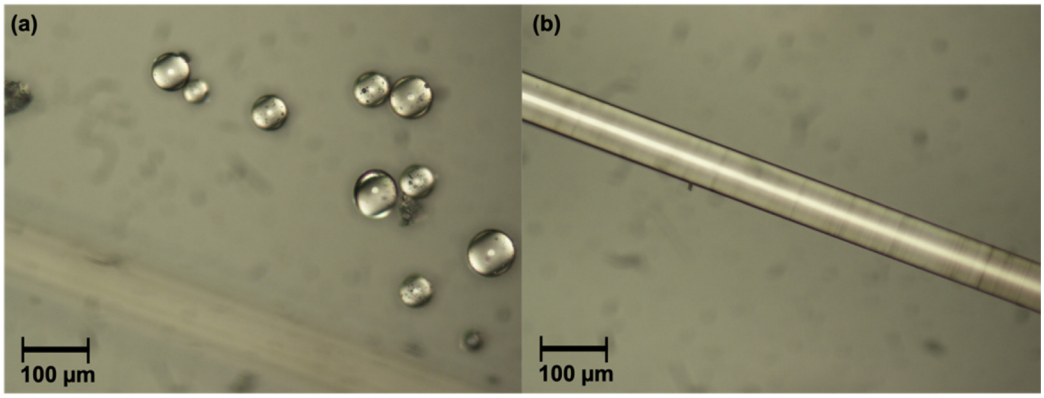

Fig. 2. Optical image of Er^{3+} doped oxyfluoride (a) microspheres with radii from 15 µm – 40 µm and (b) fiber with a radius of 41 µm used in this work.

3.3. FIR temperature correlation

The temperature correlation of the bulk glass with the intensity ratio was performed by placing the sample in the middle of a tubular horizontal oven with a thermocouple located nearest to it as possible. A continuous 532 nm DPSSL was used to excite the sample and from the other side of the oven, the emitted light was focused onto a CCD spectrograph. The emission spectra were obtained for different temperatures.

3.4. Measurement of the temperature uncertainty

In order to estimate the temperature uncertainty in the measurements using the WGM displacement technique and FIR technique, 100 spectra of the microresonators and bulk glass, were taken under the same conditions.

For the WGM displacement technique, the microsphere and fiber were first excited with a very low pump power of 3.4 mW, corresponding to room temperature, and the resonant wavelength of the WGM is taken as the reference wavelength for the succeeding measurements of wavelength displacements. The 100 spectra were taken by exciting the samples with a fixed pump power, high enough to observe the displacements of the WGM, under the same conditions. The resulting resonant wavelength displacements were correlated to the temperature. All the experiments were done inside a closed chamber in order to limit the presence of air currents, making the temperature measurements stable with time.

For the FIR technique, the 100 spectra are obtained by exciting the bulk glass inside the tubular furnace at room temperature, with a very low pump power to avoid pump-induced heating of the sample. The resulting FIR are correlated to the temperature.

The standard deviation of the temperatures is taken as the temperature uncertainty of the sample.

4. Results and discussion

4.1. Emission spectrum of erbium

In order to compare the three emission spectra of the three morphologies (microsphere, optical fiber, and bulk glass) of the Er^{3+} doped oxyfluoride glass, the spectra of the 670 nm emission band is shown in Fig. 3 for each sample. For the microsphere and fiber, the WGM resonances were observed superimposed on the Er^{3+} spectra due to the Purcell effect in which the scattered light from Er^{3+} ions is collected into the resonator modes [27]. The narrowest WGM peaks from

Optical Materials EXPRESS

the microsphere have a full width at half maximum (FWHM) of about 0.3 nm while those of the fiber have a FWHM of 0.5 nm. Narrower peaks imply higher quality factor Q [16] which suggests that the microsphere has a higher Q factor than the fiber. This disadvantage of the fiber could be attributed to its fabrication, in which the width of the fiber is not totally uniform. Therefore, the circular sections of the fiber in the detection zone may have different radius and a combination of different WGM modes is observed, broadening the observed peaks in the spectrum.

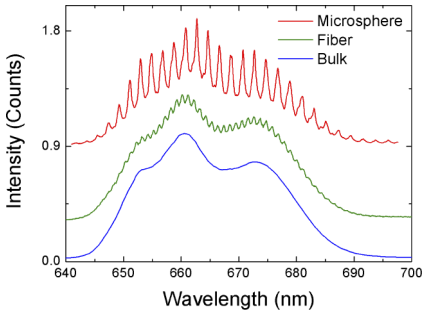

Fig. 3. The emission band at 670 nm showing the resonances associated to the WGM in the microsphere with a radius of 35 μm and fiber with a radius of 41 μm. The intensity bands were normalized and displaced vertically for comparison purposes.

Moreover, the WGM peaks can be observed in all the emission bands of the microsphere and fiber. The 670 nm ($^4F_{9/2}\rightarrow{}^4I_{15/2}$), 850 nm ($^4S_{3/2}\rightarrow{}^4I_{13/2}$), 975 nm ($^4I_{11/2}\rightarrow{}^4I_{15/2}$), and 1550 nm ($^4I_{13/2}\rightarrow{}^4I_{15/2}$) bands were used for the study of WGM displacement as a function of temperature change due to laser heating and thermal bath heating of the microsphere. For the fiber, only the 975 nm band was studied because of the low contrast of the WGM peaks.

4.2. Analysis of the WGM displacement

4.2.1. WGM displacement due to laser heating

In order to study the displacement of the WGM resonance peaks due to the heating of the microsphere and fiber with laser, five peaks from each of the emission bands were selected and their positions in each spectrum were monitored. Figure 4 is obtained by averaging the shift of these peaks for each band and spectrum.

From Fig. 4, it is clear that a general shift to the higher wavelength region of the spectra is observed as the pump power increases. The error bars were not shown because they cannot be distinguished, their height is 20 pm for the fiber and 7 pm for the microsphere (see Sect. 4.4.2). For the range of pump power considered, the experimental values show a linear tendency for each correlation suggesting that the displacement rate is independent of the pump power. A linear fitting for each emission band was done in order to calculate the average displacement rates, which is proportional to the wavelength. In the case of the 975 nm emission band of the fiber, displacement rate of 11 pm/mW was recorded while for the microsphere, displacement rates of 9 pm/mW, 11 pm/mW, 13 pm/mW, and 19 pm/mW were obtained for the 670 nm, 850 nm, 975 nm, and 1550 nm emission bands respectively. The difference between the displacement rate of the fiber and microsphere for the same 975 nm emission band is attributed to their geometry and size which result to different temperatures on the surface due to differences in heat losses when the samples were heated using the laser.

It can also be inferred from the graph that for all the emission bands, the shift does not start immediately, not until a certain pump power is applied. This shows that the heating process is not relevant until a determined pump power is reached.

Optical Materials EXPRESS

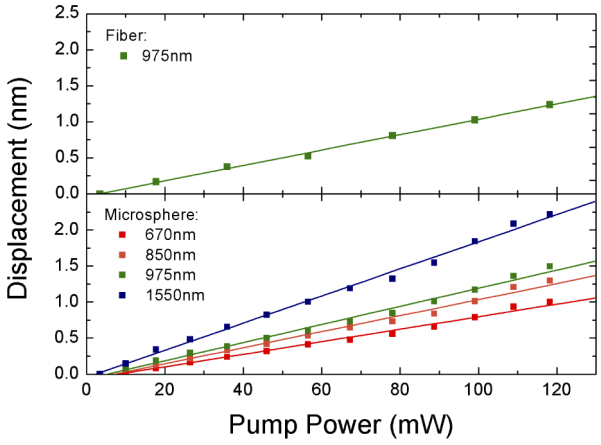

Fig. 4. Displacement of the WGM peaks of the optical fiber and microsphere as a function of the laser pump power.

4.2.2. WGM displacement due to thermal bath heating

From the measurements obtained by heating the microsphere using a thermal bath, the WGM displacements were studied as a function of temperature. For this, a data analysis similar to the procedure used in the previous section was performed for the 850 nm emission band of the microsphere and represented in Fig. 5(a). The error bars were not shown because they cannot be distinguished. Through a linear fit, the following equation was obtained: $\Delta\lambda(nm) = 0.017\ T - 5.0$, wherein 17 pm/K is the average displacement rate.

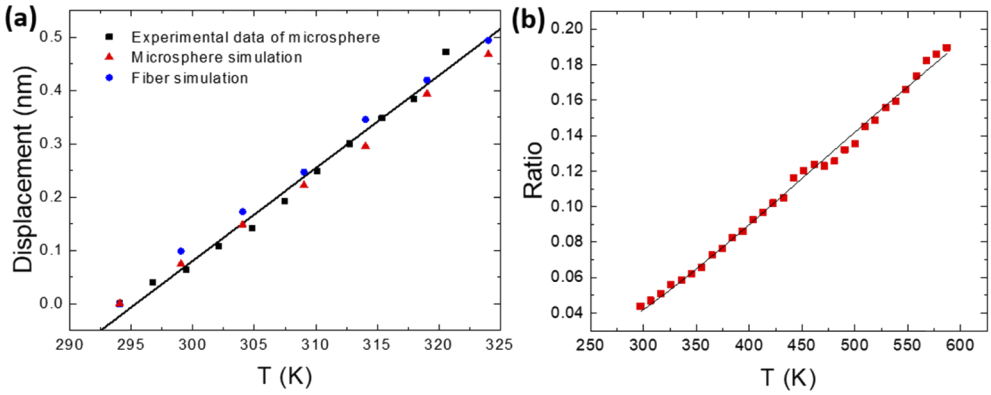

Fig. 5. (a) WGM displacement of the 850 nm band of the microsphere as a function of temperature from the experimental data (black points) with a displacement rate of 17 pm/K (black solid line). Numerical simulations of the WGM displacement in a microsphere (red points) and fiber (blue points) with displacement rates of 16 pm/K and 17 pm/K, respectively. (b) Ratio of the areas of the thermally coupled emission bands (800 nm over the 850 nm band) of Er^{3+} as a function of the bulk sample temperature. Parameters of the fit to Eq. (3) are $\Delta E = 635\ cm^{-1}$ and $B = 0.88$.

4.2.3. WGM displacement simulation as a function of temperature

The WGM in a microsphere and fiber were simulated using the Frequency Domain (ewfd) solver under the Wave Optics package of COMSOL. This solves the electromagnetic eigenfrequencies

Optical Materials EXPRESS

of the resonator modes numerically, thus, it is expected to be more precise than solving through the geometric approximation. Each sample was modeled inside a rectangular air region and an axisymmetric 2D geometry was implemented to reduce the computing time. In order to simulate the WGM, the radius and refractive index of the samples were needed. The initial radius of the microsphere and fiber models were set in accordance with those of the samples used in the experiment, 35 μm and 41 μm, respectively. A refractive index of 1.75 was used, taken from an oxyfluoride glass with similar composition in [24]. The value of the polar mode number l is set such that the resulting resonant wavelength is around the 850 nm band, permitting the comparison between the simulated and experimental results. The profile of the electric field norm of a WGM in the microsphere and fiber is represented in Fig. 6.

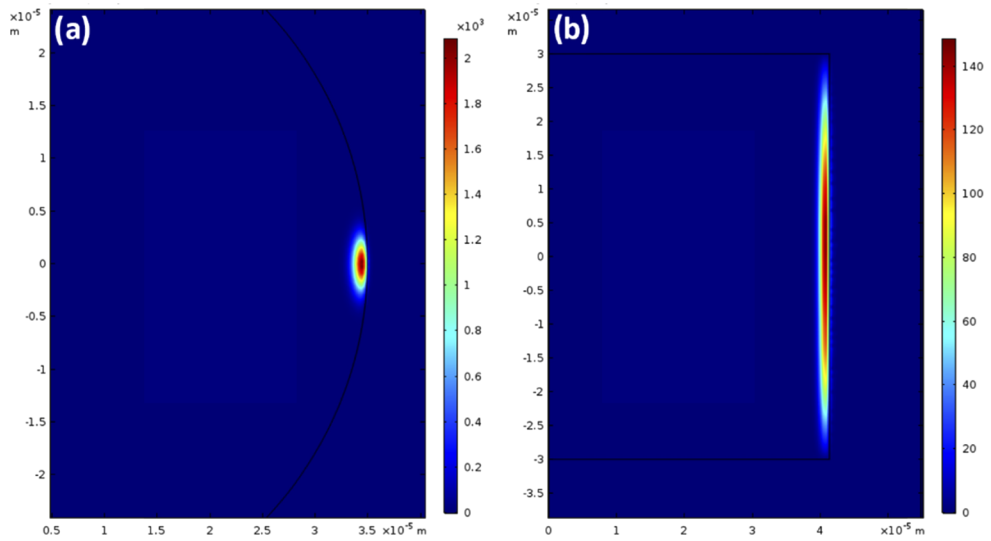

Fig. 6. Profile of the electric field norm of a WGM simulation with polarization TE of (a) microsphere: $n = 1$, $l = 435$, $m = l$ and (b) fiber: $n = 1$, $l = 516$, $m = l$; where n, l, and m are the radial, polar, and azimuthal mode number, respectively.

In order to simulate the WGM displacement with temperature, the thermal expansion coefficient α and the thermo-optic coefficient β were previously determined. Using a dilatometer and a 2 mm bulk sample of the glass, α was measured to be 13.0×10^{-6} K^{-1}. With a Michelson interferometer, the change in the optical path difference (OPD) due to α and β were measured for the same bulk sample inside a heater. This change corresponds to:

$$\Delta OPD = 2d\Delta T[(n-1)\alpha + n\beta] = N\lambda \tag{8}$$

where d and n are the thickness and the refractive index of the glass, respectively, N is the number of interference fringes for a temperature change of ΔT, and λ is the wavelength of the He-Ne laser used.

Using the previously measured value of α (13.0×10^{-6} K^{-1}), β was determined from Eq. (8) as 5.9×10^{-6} K^{-1}. Therefore, for each simulation of temperature change, the radius and refractive index of the samples were varied in accordance to the α and β of the sample. The resulting eigenfrequencies for the same resonant mode are converted to wavelength and the wavelength displacements are represented with temperature in Fig. 5(a) for the microsphere and fiber. Displacement rates with respect to temperature of 16 pm/K and 17 pm/K were obtained as the slope of the linear fit of these data, for the microsphere and fiber, respectively. As can be seen, the simulations reproduce the experimental data and show that the WGM wavelength dependence

Optical Materials EXPRESS

on temperature of both microsphere and fiber were very similar. The small difference between the simulated displacement rates for the microsphere and fiber is due to the difference in the effective refractive index of the resonant modes considered for each sample by the simulations.

The simulations were used to calculate the displacement rates with respect to temperature for the other bands of the microsphere and fiber: 13 pm/K, 19 pm/K, and 30 pm/K were obtained for the 670 nm, 975 nm, and 1550 nm bands respectively.

4.3. Fluorescence intensity ratio (FIR)

The FIR technique was used to study the behavior with temperature of an Er^{3+} doped oxyfluoride bulk glass. It consists of analyzing the ratio of the areas of the 800 nm ($^2H_{11/2}\rightarrow{}^4I_{13/2}$) and 850 nm ($^4S_{3/2}\rightarrow{}^4I_{13/2}$) emission bands as a function of the temperature of the sample. Furthermore, these bands lie within the first biological window (650 nm – 1000 nm), thus a thermal correlation of these bands can have various biomedical applications [28]. Figure 5(b) shows the experimental values obtained for the ratio at certain temperatures. The error bars were not shown because they cannot be distinguished (see Sect. 4.4.2). It can be observed that as the temperature rises, the area of the 800 nm band also increases with respect to that of the 850 nm band. This verifies that as the temperature increases, the vibration of the phonons in the host material increases and they interact with the erbium ions in order to promote the ones from the $^4S_{3/2}$ level to the $^2H_{11/2}$ level, thus, increasing the 800 nm band intensity with respect to the 850 nm band. The experimental values were then fitted to a Boltzmann distribution (see Eq. (3)) and an energy gap of 635 cm^{-1} was obtained.

4.4. Sensor performance of the microsphere, fiber, and bulk glass

4.4.1. Relative sensitivity

The variation of the WGM wavelength with temperature can be obtained from Fig. 5(a) as the slope of the linear fit expressed as $(\alpha+\beta)\lambda$. This slope allows the estimation of the relative sensitivity, which for the 850 nm band of the microsphere has a value of 2.0×10^{-5} K^{-1}. Since α and β do not depend on the wavelength, according to Eq. (5), the relative sensitivity is also independent of the wavelength, thus, the same relative sensitivity will be obtained for the rest of the emission bands of the microsphere. Moreover, as α and β are also independent of the morphology of the material, the fiber has the same relative sensitivity as the microsphere. For comparison, a relative sensitivity of 5.3×10^{-6} K^{-1} was observed for a silica fiber as reported in [10].

The relative sensitivity of the bulk glass using the FIR technique is calculated using the fitted parameters of Fig. 5(b) through Eq. (6). The maximum sensitivity was obtained for the lowest temperature being 1.0×10^{-2} K^{-1}. This is similar to the sensitivity measured in an Er^{3+}/Yb^{3+} doped $LaGdO_3$ glass as reported in [14]. It can be seen that the bulk glass has a significantly higher value of sensitivity than the microresonators.

4.4.2. Temperature uncertainty

Temperature uncertainties for the WGM and FIR techniques were experimentally estimated by measuring 100 spectra under the same experimental conditions. In the case of the WGM technique, the position of a WGM peak was estimated for each of the 100 spectra (both for the microsphere and the fiber) by calculating the centroid of the WGM peak. The distribution of the centroid positions for the microsphere was represented in Fig. 7. The peak position uncertainty $\delta\lambda$ was taken as the standard deviation and is 0.007 nm for the microsphere and 0.020 nm for the fiber. The uncertainty in the WGM position of the microsphere is lower compared to that of the fiber because of its higher Q factor as mentioned before. A similar order of magnitude is predicted by Vollmer and Arnold in which the uncertainty in the WGM position of the microsphere is about 1% of the FWHM of the peak [29].

Optical Materials EXPRESS

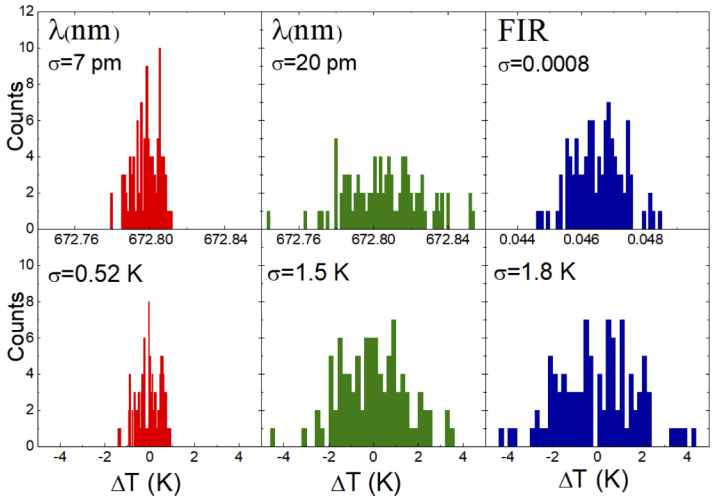

Fig. 7. Distribution of the measured parameters (i.e. wavelength, ratio) for microsphere (red), fiber (green) and bulk glass (blue), the corresponding temperature distribution obtained from the WGM displacement analysis and FIR technique for the three samples.

The temperatures corresponding to the WGM peak position of the microsphere and fiber were estimated from the correlation for each of the 100 measurements and the resulting temperature distribution is represented in Fig. 7. The temperature uncertainty was estimated as the standard deviation of the temperature distribution having a value of 0.52 K for the microsphere and 1.5 K for the fiber, both corresponding to the 670 nm band.

In the case of the FIR technique, the distribution of intensity ratios of the 100 measured spectra was obtained and represented in Fig. 7, as well as the temperature distribution inferred from the correlation curve. The uncertainty in the ratio of intensities δFIR is 8.0×10^{-4} and the resulting temperature uncertainty is 1.8 K.

As can be seen from Fig. 7, the distribution of temperature is significantly narrower in the case of the WGM technique of the microsphere.

Temperature uncertainties for the rest of emission bands of the microsphere and fiber were estimated from the value obtained for the 670 nm band using Eq. (7). The temperature uncertainties obtained for the 850 nm, 975 nm, 1550 nm band were 0.41 K, 0.36 K, and 0.22 K respectively for the microsphere, and 1.2 K, 1.0 K, and 0.65 K respectively for the fiber. In first approximation, it can be said that the formation due to surface tension of the microsphere has no effect on it having minimal temperature uncertainty since the internal stress originated in such a small volume and therefore negligible. Moreover, although the calculations show that the temperature uncertainty of the microresonators decreases with increasing wavelength, the resolutions of equipment when detecting in the visible region is generally better than in the NIR region and must also be taken into consideration.

The sensor parameters obtained for the three forms of Er^{3+} doped oxyfluoride glass are summarized in Table 1. A similar temperature uncertainty for WGM ($\delta T = 0.1$ K) and FIR ($\delta T = 1$ K) were estimated in the literature [9] for a Nd^{3+} doped barium titano silicate microsphere and bulk glass. It can be observed that the relative sensitivity of the WGM based sensors (i.e. microsphere and fiber) are three orders of magnitude lower than that of the FIR based sensor (i.e. bulk glass). However, the temperature uncertainty from the WGM analysis of microsphere is approximately three times lower than that obtained by the fiber and bulk glass. Therefore, the microsphere is considered the best choice since it provides the most precise temperature measurements among the three morphologies.

Optical Materials EXPRESS

Table 1. Sensor parameters of the three morphologies of Er^{3+} doped oxyfluoride glass

Sensor Parameter	Microsphere	Optical Fiber	Bulk Glass
Relative sensitivity (K^{-1})	2.0×10^{-5}	2.0×10^{-5}	1.0×10^{-2}
Temperature uncertainty (K)			1.8
670 nm	0.52	1.5	
850 nm	0.41	1.2	
975 nm	0.36	1.0	
1550 nm	0.22	0.65	

5. Conclusions

Through this work, the thermal sensing capabilities of three morphologies of Er^{3+} doped oxyfluoride glass were characterized using a WGM displacement analysis and FIR technique and comparisons of each performance were made. From the 850 nm band of the microsphere, the displacement rate as a function of temperature was also obtained to be 17 pm/K for the 850 nm band. The α and β of a bulk glass sample were measured independently from the WGM phenomenon and the obtained values were used in the numerical simulations of the WGM displacements with temperature. The simulations for both the microsphere and fiber were successfully used to reproduce the experimental results. Through the FIR technique, an energy gap of 635 cm^{-1} was estimated between the thermally coupled levels $^2H_{11/2}$ and $^4S_{3/2}$. The relative sensitivity of the bulk glass was found to be three orders of magnitude greater than that of the microsphere, while the temperature uncertainty obtained was three times higher. This implies more precise measurements of temperature using WGM analysis of microsphere compared with the fiber and the FIR technique of the bulk glass.

Funding

Ministerio de Economía y Competitividad (FIS2016-77319-C2-1-R, MAT2015-71070-REDC, MAT2016-75586-C4-4-P); Agencia Estatal de Investigación (IJCI-2016-30498); European Regional Development Fund.

References

1. A. Rostami, H. Ahmadi, H. Heidarzadeh, and A. Taghipour, "Microsphere and Fiber Optics based Optical Sensors," Opt. Sensors - New Dev. Pract. Appl. (2014).
2. V. K. Rai, "Temperature sensors and optical sensors," Appl. Phys. B: Lasers Opt. **88**(2), 297–303 (2007).
3. N. M. Hanumegowda, I. M. White, and X. Fan, "Aqueous mercuric ion detection with microsphere optical ring resonator sensors," Sens. Actuators, B **120**(1), 207–212 (2006).
4. M. Bass and W. Koechner, *Solid-State Lasers: A Graduate Text* (Springer, 2002).
5. S. Tanabe, "Optical transitions of rare earth ions for amplifiers: How the local structure works in glass," J. Non-Cryst. Solids **259**(1-3), 1–9 (1999).
6. S. Tanabe, H. Hayashi, T. Hanada, and N. Onodera, "Fluorescence properties of Er3+ ions in glass ceramics containing LaF3 nanocrystals," Opt. Mater. (Amsterdam, Neth.) **19**(3), 343–349 (2002).
7. L. Feng, J. Wang, Q. Tang, L. Liang, H. Liang, and Q. Su, "Optical properties of Ho3+-doped novel oxyfluoride glasses," J. Lumin. **124**(2), 187–194 (2007).
8. L. de Sousa-Vieira, S. Ríos, I. R. Martín, L. García-Rodríguez, V. N. Sigaev, V. I. Savinkov, and G. Y. Shakhgildyan, "Whispering gallery modes in a holmium doped glass microsphere: Temperature sensor in the second biological window," Opt. Mater. (Amsterdam, Neth.) **83**, 207–211 (2018).
9. L. L. Martín, C. Pérez-Rodríguez, P. Haro-González, and I. R. Martín, "Whispering gallery modes in a glass microsphere as a function of temperature," Opt. Express **19**(25), 25792 (2011).
10. E. Rivera-Pérez, I. L. Villegas, A. Díez, M. V. Andres, J. L. Cruz, and A. Rodríguez-Cobos, "Measurement of pump-induced temperature increase in doped fibers using whispering-gallery modes," IEEE Photonics Technol. Lett. **25**(24), 2498–2500 (2013).
11. H. Guo, F. Pang, X. Zeng, N. Chen, Z. Chen, and T. Wang, "Temperature sensor using an optical fiber coupler with a thin film.," Appl. Opt. **47**(19), 3530–3534 (2008).

Optical Materials EXPRESS

12. C. Pérez-Rodríguez, L. L. Martín, S. F. León-Luis, I. R. Martín, K. K. Kumar, and C. K. Jayasankar, "Relevance of radiative transfer processes on Nd3+ doped phosphate glasses for temperature sensing by means of the fluorescence intensity ratio technique," Sens. Actuators, B **195**, 324–331 (2014).
13. S. A. Wade, "Temperature Measurement Using Rare Earth Doped Fibre Fluorescence," (1999).
14. A. Siaï, P. Haro-González, K. Horchani Naifer, and M. Férid, "Optical temperature sensing of Er3+/Yb3 + doped LaGdO3based on fluorescence intensity ratio and lifetime thermometry," Opt. Mater. **76**, 34–41 (2018).
15. T. J. A. Kippenberg, "Nonlinear Optics in Ultra-high-Q Whispering-Gallery Optical Microcavities," Thesis (2004).
16. G. C. Righini, Y. Dumeige, P. Féron, M. Ferrari, G. N. Conti, D. Ristic, and S. Soria, "Whispering Gallery Mode microresonators: Fundamentals and applications," Riv. del Nuovo Cim. **34**(7), 435–488 (2011).
17. T. Ioppolo and M. V. Ötügen, "Pressure tuning of whispering gallery mode resonators," J. Opt. Soc. Am. B **24**(10), 2721 (2007).
18. L. Labrador-Páez, K. Soler-Carracedo, M. Hernández-Rodríguez, I. R. Martín, T. Carmon, and L. L. Martin, "Liquid whispering-gallery-mode resonator as a humidity sensor," Opt. Express **25**(2), 1165 (2017).
19. G. Ghosh, "Model for the Thermooptical Coefficients of Some Standard Optical-Glasses," J. Non-Cryst. Solids **189**(1-2), 191–196 (1995).
20. D. S. Sanditov and B. S. Sydykov, "Modulus of elasticity and thermal expansion coefficient of glassy solids," Phys. Solid State **56**(5), 1006–1008 (2014).
21. S. F. Collins, G. W. Baxter, S. A. Wade, T. Sun, K. T. V. Grattan, Z. Y. Zhang, and A. W. Palmer, "Comparison of fluorescence-based temperature sensor schemes: Theoretical analysis and experimental validation," J. Appl. Phys. **84**(9), 4649–4654 (1998).
22. C. D. S. Brites, A. Millán, and L. D. Carlos, "Lanthanides in Luminescent Thermometry," Handb. Phys. Chem. Rare Earths **49**, 339–427 (2016).
23. J. Mendez-Ramos, V. Lavin, I. R. Martin, U. R. Rodriguez-Mendoza, J. A. Gonzalez-Almeida, V. D. Rodriguez, A. D. Lozano-Gorrin, and P. Nunez, "Optical properties of Er 3+ ions in transparent glass ceramics," J. Alloys Compd. **323-324**, 753–758 (2001).
24. P. A. Tick, N. F. Borrelli, L. K. Cornelius, and M. A. Newhouse, "Transparent glass ceramics for 1300 nm amplifier applications," J. Appl. Phys. **78**(11), 6367–6374 (1995).
25. G. R. Elliott, D. W. Hewak, G. S. Murugan, and J. S. Wilkinson, "Chalcogenide glass microspheres; their production, characterization and potential," Opt. Express **15**(26), 17542–17553 (2007).
26. L. L. Martín, P. Haro-González, I. R. Martín, D. Navarro-Urrios, D. Alonso, C. Pérez-Rodríguez, D. Jaque, and N. E. Capuj, "Whispering-gallery modes in glass microspheres: optimization of pumping in a modified confocal microscope," Opt. Lett. **36**(5), 615 (2011).
27. T. J. Kippenberg, A. L. Tchebotareva, J. Kalkman, A. Polman, and K. J. Vahala, "Purcell-factor-enhanced scattering from Si nanocrystals in an optical microcavity," Phys. Rev. Lett. **103**(2), 027406 (2009).
28. H. Suo, F. Hu, X. Zhao, Z. Zhang, T. Li, C. Duan, M. Yin, and C. Guo, "All-in-one thermometer-heater up-converting platform YF_3:Yb^{3+}, Tm^{3+} operating in the first biological window," J. Mater. Chem. C **5**(6), 1501–1507 (2017).
29. F. Vollmer and S. Arnold, "Whispering-gallery-mode biosensing: Label-free detection down to single molecules," Nat. Methods **5**(7), 591–596 (2008).